

# Microstructure investigation of Ni<sub>3</sub>Al intermetallic alloy coating on AISI 304 steel by PTA process

BULENT KURT\*

*Nevsehir Hacı Bektaş Veli University, Faculty of Engineering and Architecture, Department of Metallurgy and Materials Engineering, Nevsehir/Turkey*

In this study, AISI 304 austenitic stainless steel was coated with Ni<sub>3</sub>Al intermetallic alloy. Coating layers were formed at 110, 120 and 130 A currents values by plasma transfer arc (PTA) process with using argon gas for both plasma and protective. Analyses of microhardness, SEM, EDX and XRD were carried out in order to examine surface and interface characteristics of the coating layers. From the results, it was found that the primer Ni<sub>3</sub>Al phase and secondary NiAl phase existed in the Ni<sub>3</sub>Al alloy coating obtained by PTA process at 110 A current. From the results, it was seen that increased current values caused to the cracks in the coating layer and also affected the coating layer and interface microstructure.

(Received April 29, 2014; accepted January 21, 2015)

*Keywords:* PTA coating, Ni<sub>3</sub>Al, Microstructure, Austenitic stainless steel

## 1. Introduction

The demands on the lifetime and surface performance of the materials are continuously increasing. Thus, different surface coating techniques have been used to improve surface properties of materials. Surface properties and quality depend strongly upon the selected alloys and deposition processes [1-5]. The use of plasma transferred arc technique for deposition of high-performance coatings has been attempted by many researchers [6-9]. Fabricating high, wear-resistant coatings on their surfaces is an efficient approach to improve the surface properties of metallic material without affecting seriously the properties of the substrate materials. [10-12]. Plasma transferred arc (PTA) process can be defined as a gas-shielded arc welding process where the coalescence of metals is achieved via the heat transferred by an arc that is created between a tungsten electrode and a submaterial. The arc is constricted by a copper alloy nozzle orifice to form a highly collimated arc column. The plasma is formed through the ionization of a portion of the plasma (orifice) gas [13].

Ni<sub>3</sub>Al has excellent corrosion and oxidation resistance in a wide range of temperatures owing to formation of highly stable alumina oxide layer on the surface. Also, Ni<sub>3</sub>Al keeps its phase stability up to high temperatures close to its melting point [14]. Austenitic stainless steel is a widely used engineering alloy in liquid-handling systems and hydraulic machinery because of its excellent corrosion resistance, good processibility, and relatively low cost. However, they exhibit high toughness and good oxidation resistance only up to the temperatures of nearly 600 °C [15,16].

In this paper, PTA weld-surfacing process was adopted to produce composite coating on AISI 304

stainless steel substrate using Ni<sub>3</sub>Al intermetallic alloy. Microstructural characteristics of the coating layer and the interface of Ni<sub>3</sub>Al intermetallic alloy and stainless steel were characterized using scanning electron microscopy (SEM), X-ray analysis (EDS), X-ray diffraction (XRD) and energy dispersive analysis and microhardness measurements.

## 2. Experimental procedure

In this study, Ni<sub>3</sub>Al intermetallic alloy rod of 2 mm diameter and the AISI 304 stainless steel flat bar of 10 mm thick were used as coating and substrate material respectively. AISI 304 Stainless steel specimens were cut to the dimensions 80 × 25 × 10 mm<sup>3</sup>, polished with 220-grit SiC abrasive paper and rinsed with ethyl alcohol prior to coating. Table 1 shows the chemical compositions of the materials. The operating principle of PTA process is schematically shown in Fig. 1. Surface coating procedure was realized that different three current values were used. Parameters of PTA weld-surfacing process are given in Table 2.

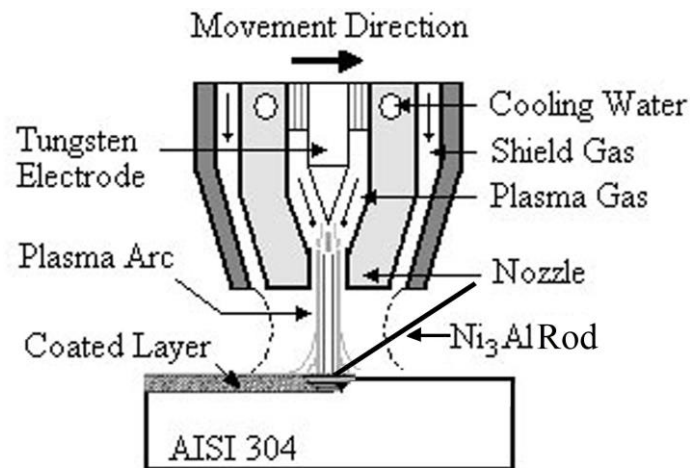


Fig. 1. Schematic appearance of PTA coating method.

Table 1. Chemical compositions of the coating and substrate materials.

Alloy	Composition (%)									
	C	Cr	Ni	Mo	Si	Mn	P	S	Al	Fe
Ni <sub>3</sub> Al	0.007	0.046	Bal	0.002	0.03	0.024	0.002	0.0004	11.12	0.45
AISI 304	0.02	17.3	11.0	2.2	0.78	1.8	0.02	0.015	-	Bal.

Table 2. PTA weld-surfacing process experimental parameters.

Arc current (A)	110 - 120 - 130
Shield gas flow (Ar, l/min)	25
Plasma gas flow (Ar, l/min)	0,2
Diameter of electrode (mm)	4,7
Travel speed (mm/s)	2,2
Torch gap (mm)	3

When the plasma arc transferred the surface of the specimen, the coating material was melted simultaneously and melted coating layer occurred on the substrate material surface. Thus, a novel coating layer, which is metallurgically bonded to substrate and has rapidly solidified microstructure, was fabricated.

Metallographic examination of the coating layer and, the interface of coating layer and substrate material involved preparing transverse sections followed by grinding and polishing to 3  $\mu$ m diamond paste. For

microstructural examination, the specimens were etched electrolytically in a solution of 50 ml HNO<sub>3</sub> and 50 ml pure water. The microstructures of the specimens were investigated by scanning electron microscopy (SEM), the energy dispersive X-ray (EDX) and XRD analysis. Microhardness measurements were carried out by a Leica microhardness tester under a load of 50 g.

### 3. Results and discussions

Fig. 2 shows the typical surface microstructure of the alloyed layers with three different currents values. It can be seen that the width of effective coating layers is 1.2, 1.8 and 2.6 mm at 110, 120 and 130 A respectively. Increasing current values were caused to higher mix ratio between alloyed layer and substrate material. No cracks or pores were seen both in the alloyed layer and interface at the 110 A current (It is clearly seen in Fig. 2 a). But, the microcracks caused at the coated layers with increasing arc current value. It is clearly seen in Fig. 2 (b) and Fig. 2(c). This can be attributed to a combination of factors; including high thermal residual stresses under rapid solidification and high temperature non-equilibrium phases generated [17].

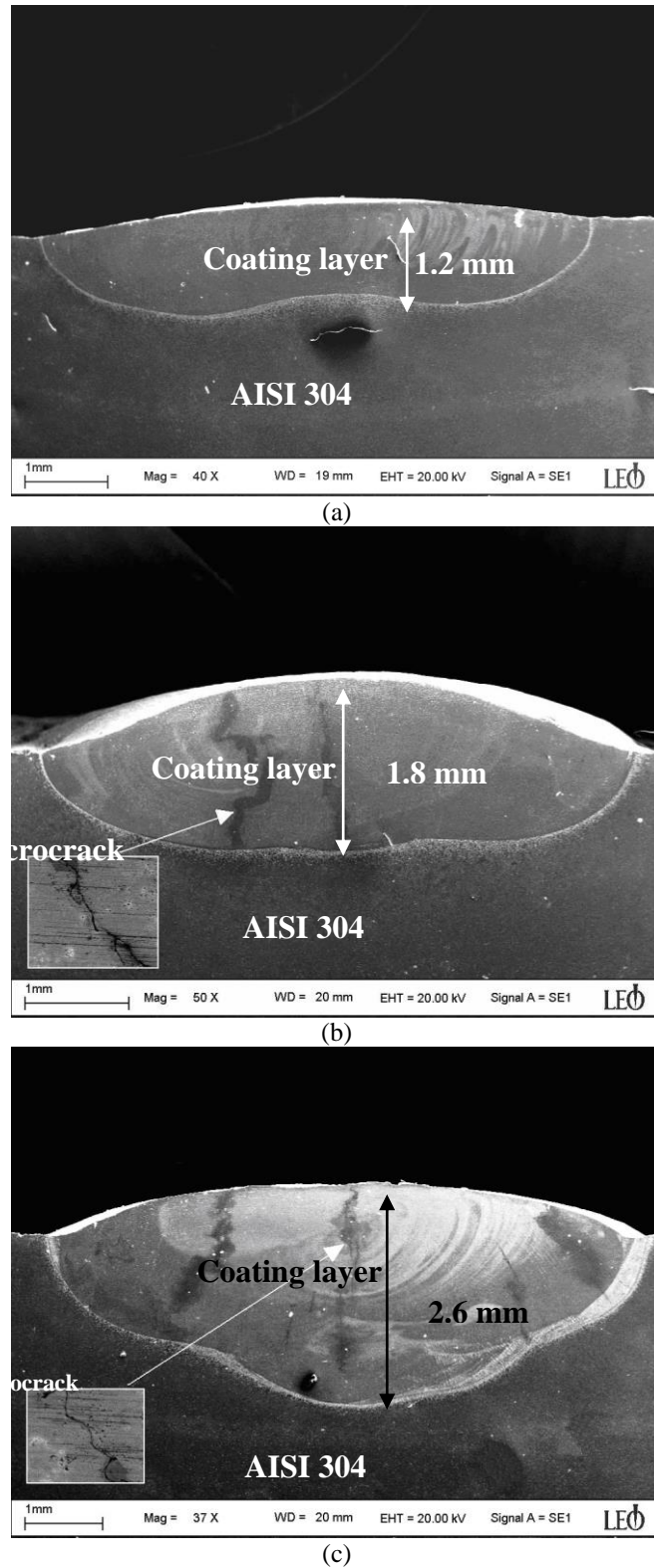
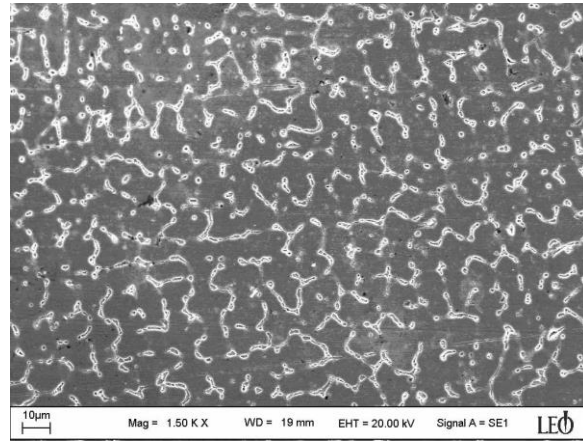
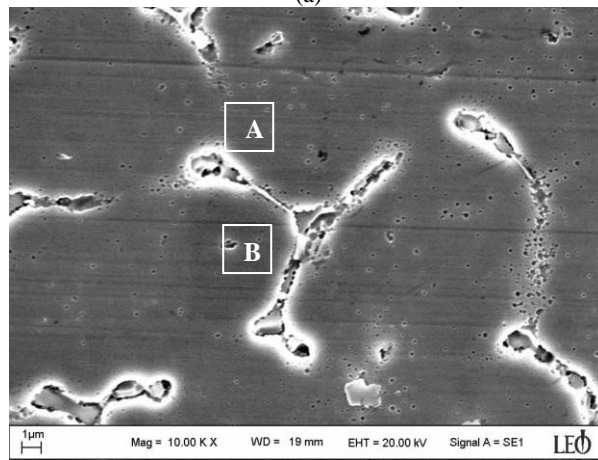


Fig. 2. SEM micrographs of coating layer depths at the 110 A (a), 120 A (b) and 130 A (c) currents.

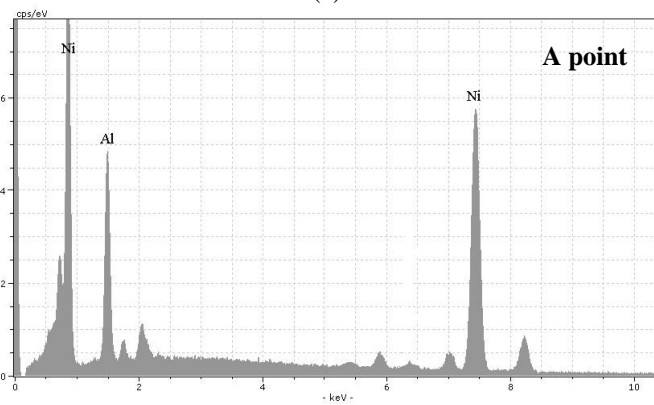
Fig. 3 shows SEM image of the etched cross-section of the  $\text{Ni}_3\text{Al}$  intermetallic alloy deposited by the PTA process at 110 A current value.



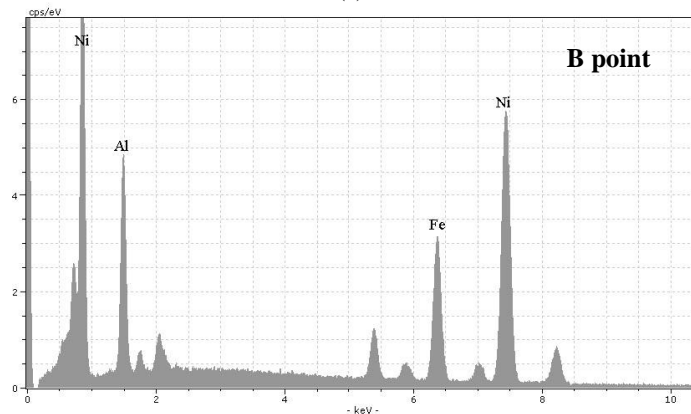
(a)



(b)



(c)



(d)

Fig. 3. SEM micrograph of coating layer at the 110 A.

From the Fig. 3 (a), two different phases are seen as matrix and precipitate phases. This situation clearly is shown at the magnified micrograph in the Fig. 3 (b). The EDX results taken from A and B points in Fig. 3 (b) are shown in Fig. 3 (c) and (d). The composition of alloyed layer main material consists of 84.4 % Ni, 14.6 % Al and 0.55 % Fe. From the Ni-Al binary phase diagram, thus compositions were determined as  $\text{Ni}_3\text{Al}$  phase for A point and NiAl phase for B point. The precipitate phase composition into the coating layer was determined as 70.2 % Ni, 24.4 % Al and 4.8 % Fe from the EDX result. The NiAl phase with small volume fraction is distributed non-uniformly in the  $\text{Ni}_3\text{Al}$  matrix. This phase was also caused to relatively smaller grain size. Fig. 4(a) shows the microstructure of the alloyed layer using 120 A current. When the employed arc current reaches 120 A, precipitated phases are dispersed into the coating layer matrix and its

contents are decreased. This situation can be clarified by increasing heat input and mixed alloying elements from the AISI 304 stainless steel. The matrix phase for 120 A current consist of 55.4 % Ti, 29.5 % Fe, 7.5 % Cr and 7.6 % Al from EDX analysis taken in this field (Fig. 4 (b)). This composition was determined to be  $\gamma$  phase by Fe-Cr-Ni ternary phase diagram. This result showed that in the high currents as 120 A,  $\text{Ni}_3\text{Al}$  intermetallic alloy not formed. Fig. 5(a) and (b) shows the microstructure of alloyed layer for 120 A. The interface micrographs of the alloyed layer and substrate material are seen in Fig. 6. The width of the interface zone, which formed with rapid solidification, was 5  $\mu\text{m}$  for 120 A and 10  $\mu\text{m}$  for the currents of 130 A (Fig. 6(b) and Fig. 6(c)). The width of heat affected zones (HAZ) was approximately 40  $\mu\text{m}$ , 60  $\mu\text{m}$  and 90  $\mu\text{m}$  for 110, 120 and 130 A respectively.

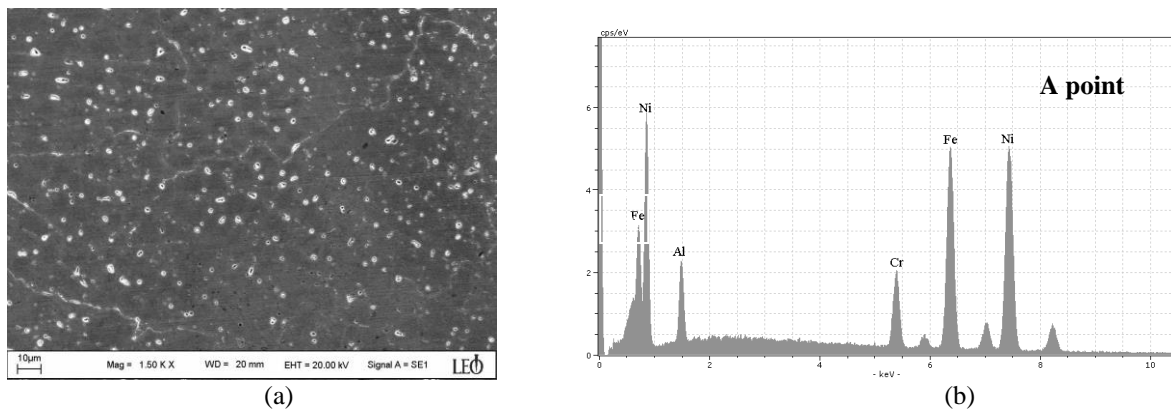


Fig. 4. SEM micrograph of coating layer at the 120 A.

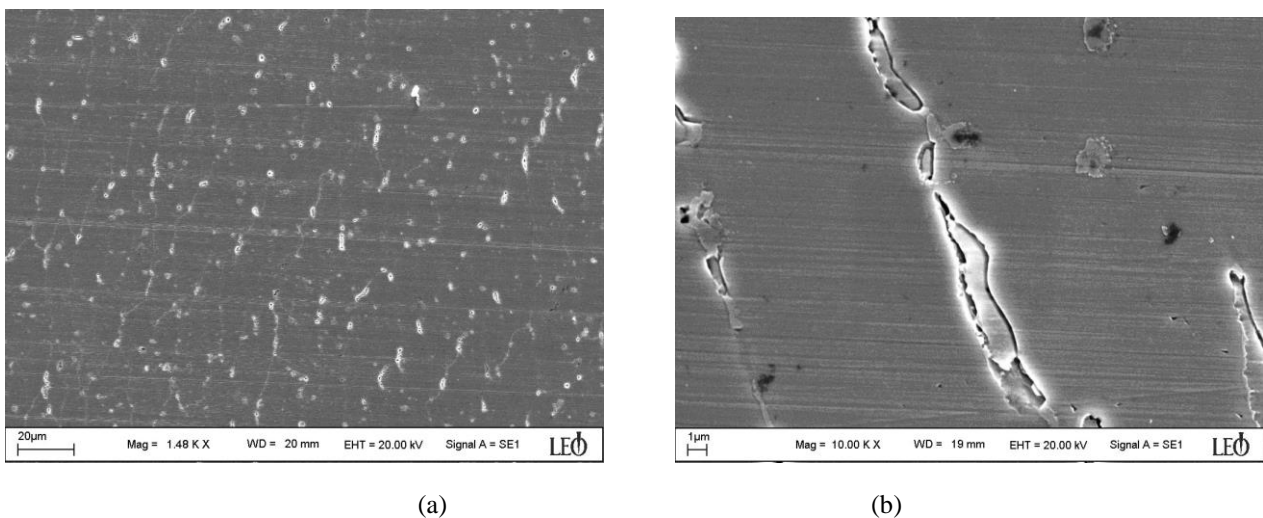
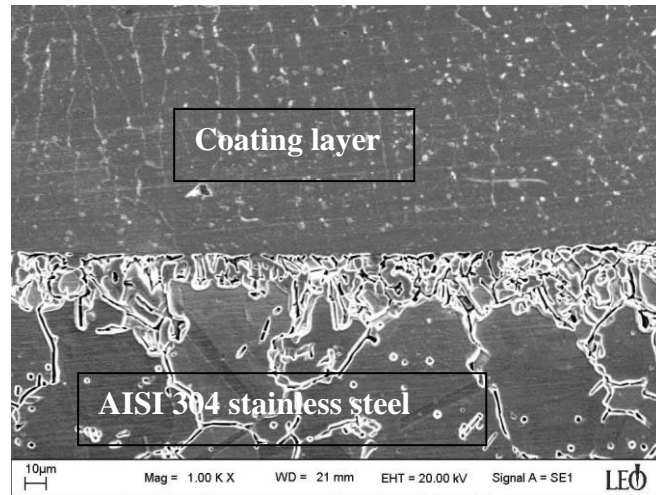
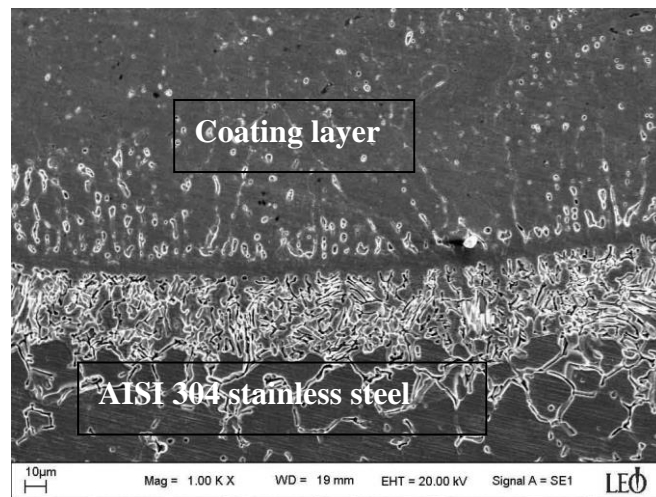


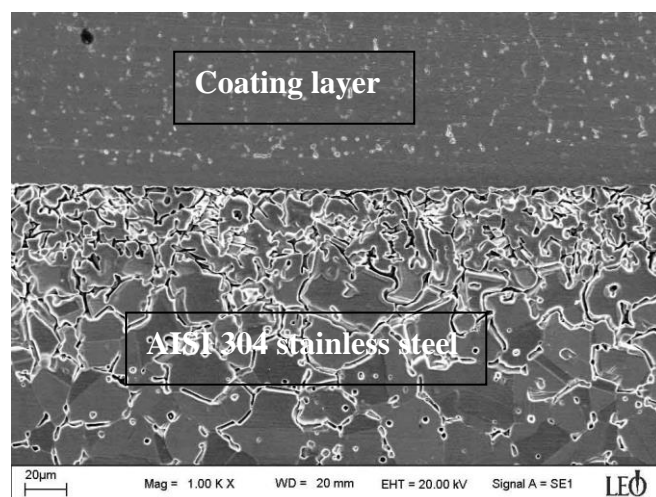
Fig. 5. SEM micrograph of coating layer at the 130 A.



(a)



(b)



(c)

Fig. 6. SEM micrograph of coating layer and substrate material interface at at the 110 A (a), 120 A (b) and 130 A (c) currents.

The XRD pattern of the Ni<sub>3</sub>Al coating layer at the 110 A is shown in Fig. 7. The desired product Ni<sub>3</sub>Al is the predominant phase in the alloyed layer. In addition, NiAl phase was formed in the coating layer as second phase. This result also supported the microstructural results.

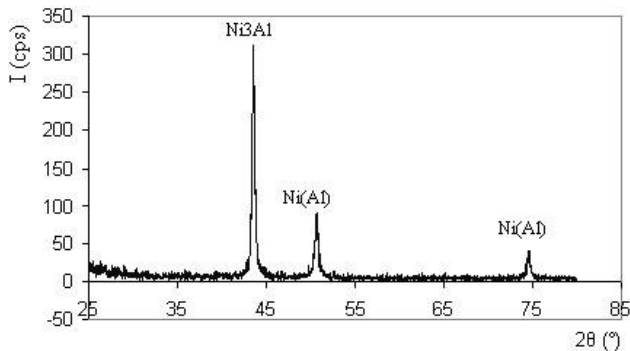


Fig. 7. X-ray profile of the Ni<sub>3</sub>Al coating layer for 110 A.

The microhardness test results taken from the coating layer surface towards substrate material are shown in Fig. 8. From the figure it is clearly shown that increased welding currents reduce the coating layer hardness. This result can be explained with increased heat input according to increased welding currents. Increased heat input caused to higher mixture ratio between coating and substrate materials. Therefore, increased Fe and Cr addition reduced the hardness of coating layer. From the coating layer microstructure and EDX result in Fig. 4 it is clearly shown that higher heat input caused to  $\gamma$  phase formation in the coating layer.

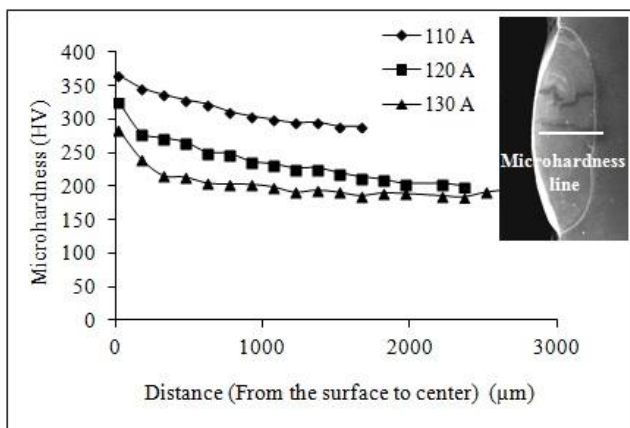


Fig. 8. Microhardness distribution from the coating layer surface to the substrate material.

#### 4. Conclusions

Ni<sub>3</sub>Al intermetallic alloy was coated on AISI 304 austenitic stainless steel surface by plasma transfer arc (PTA) process. The following results were obtained.

- 1- The coating layer thickness of 1.2, 1.8 and 2.6 mm at 110, 120 and 130 A currents, respectively were obtained.
- 2- Microcracks in the coating layer occurred at the 120 and 130 A current values. This can be high thermal residual stresses under rapid solidification and high temperature non-equilibrium phases generated.
- 3- In the increased currents, Ni<sub>3</sub>Al intermetallic alloy not formed.
- 4- The microhardness of coating layers decreased with the increased current values.

#### References

- [1] R. Iakovou, L. Bourithis, G. Papadimitriou, *Wear*; **252**, 1007 (2002).
- [2] R. L. Deuis, J. M. Yellup, C. Subramanian, *Composites Science and Technology*; **58**, 299 (1998).
- [3] Y.-F. Liu, J.-M. Han, R.-H. Li, W.-J. Li, X.-Y. Xu, J.-H. Wang, S.-Z. Yang, *Applied Surface Science*; **252**, 7539 (2006).
- [4] F.-Y. Hung, Z.-Y. Yan, L.-H. Chen, T.-S. Lui, *Surface and Coatings Technology*; **200**, 6881 (2006).
- [5] J. B. Cheng, B. S. Xu, X. B. Liang, Y. X. Wu, *Materials Science and Engineering: A* **492**, 2008 (407).
- [6] J. Cheng, B. Xu, X. Liang, Y. Wu, Z. Liu, *Material*, **15**, 451 (2008).
- [7] L. Bourithis, G. D. Papadimitriou, *Materials Science and Engineering A* **361**, 165 (2003).
- [8] L. Zhang, B. Liu, H. Yu, D. Sun, *Surface and Coatings Technology* **201**, 5931 (2007).
- [9] E. Bourithis, A. Tazedakis, G. Papadimitriou, *Journal of Materials Processing Technology*, **128**, 169 (2002).
- [10] R. R. Bharath, R. Ramanathan, B. Sundararajan, P. B. Srinivasan, *Materials & Design*, **29:9**, 1725 (2008).
- [11] L. Bourithis, S. Papaefthymiou, G. D. Papadimitriou, *Applied Surface Science*, **200**, 203 (2002).
- [12] H.-J. Kim, B.-H. Yoon, C.-H. Lee, *Wear*; **249**, 846 (2001).
- [13] I. D. Harris, *ASM Metals Handbook*, **6**, (Materials Park, OH, 1993), pp. 195.
- [14] Y. Nunomura, Y. Kaneno, H. Tsuda, T. Takasugi, *Intermetallics* **12**, 389 (2004).
- [15] M. W. Mahoney, C. C. Bampton, *ASM handbook*, **6**, (Materials Park, OH, 1993), pp.156.
- [16] J. A. Brooks, J. C. Lippold, *ASM Metals Handbook*, Volume 6, (Materials Park, OH, 1993), pp. 500-504.
- [17] S. Buytoz, *Surface and Coatings Technology*, **200**, 3734 (2006).

\*Corresponding author: bkurt@nevsehir.edu.tr